

Optomechanical System Design for Dual-Mode Stand-Off Submillimeter Wavelength Imagers

Gandini, Erio; Svedin, Jan; Bryllert, Thomas; Llombart Juan, Nuria

DOI

[10.1109/TTHZ.2017.2700759](https://doi.org/10.1109/TTHZ.2017.2700759)

Publication date

2017

Document Version

Accepted author manuscript

Published in

IEEE Transactions on Terahertz Science and Technology

Citation (APA)

Gandini, E., Svedin, J., Bryllert, T., & Llombart Juan, N. (2017). Optomechanical System Design for Dual-Mode Stand-Off Submillimeter Wavelength Imagers. *IEEE Transactions on Terahertz Science and Technology*, 7(4), 393-403. Article 7929367. <https://doi.org/10.1109/TTHZ.2017.2700759>

Important note

To cite this publication, please use the final published version (if applicable). Please check the document version above.

Copyright

Other than for strictly personal use, it is not permitted to download, forward or distribute the text or part of it, without the consent of the author(s) and/or copyright holder(s), unless the work is under an open content license such as Creative Commons.

Takedown policy

Please contact us and provide details if you believe this document breaches copyrights. We will remove access to the work immediately and investigate your claim.

Opto-Mechanical System Design for Dual-Mode Stand-Off Submillimeter wavelength Imagers

Erio Gandini, Jan Sevedin, Tomas Bryllert, and Nuria Llombart

Abstract—In this contribution, the practical trade-offs for designing submillimeter wavelength imagers based on opto-mechanical systems combined with focal plane arrays are presented. The architecture of these systems differs for operation at short and long ranges. General formulas to derive the effective field of view of diffraction limited quasi-optical systems in these two scenarios are shown. These formulas can be used to evaluate the performance of a specific optical system implementation. As an application example, we present the design of an opto-mechanical system that can operate at both ranges in a modular approach. The presented implementation achieves an effective field of view which is 70% of the canonical one. The proposed solution consists of a linear focal plane array of eight active transceivers combined with a raster scan technique. The system for short range scenario is a side-fed dual-reflector Dragonian architecture because of its good scanning performance when illuminated by a focal plane array. Thanks to the small system aperture, the scanner is arranged after the primary mirror, without causing additional scan loss. The Dragonian system is then used to illuminate a confocal dual-reflector architecture for the long range scenario. The scanner in this case is before the main aperture and it has to be considered in the performance optimization of the optical system since it adds phase aberration loss.

Index Terms—Sub-millimeter wavelength, quasi-optical system, opto-mechanical system, stand-off detection, imaging system, concealed object detection, security.

I. INTRODUCTION

SECURITY imagers for concealed object detection are key devices to guarantee the security of public spaces such as airports, military compounds and venues. Concealed weapon detection has been achieved in several frequency bands [1]–[3]. X-ray imagers are widely used for screening of luggage [1]. However, X-radiation is ionizing and therefore may cause health risks. For this reason, these imagers have been prohibited by the European Community for people screening. Instead, millimeter wavelength imagers, based on synthetic imaging techniques combined with a portal like configuration, are nowadays successfully being used in many airports worldwide [2]. The extension of these systems at large distances is challenging since large antenna apertures would be needed

E. Gandini, Nuria Llombart are with the department of Electrical Engineering, Mathematics and Computer Science of Delft University of Technology, Delft, The Netherlands (e-mail: E.Gandini, N.Llombart@tudelft.nl). Jan Sevedin is with the Swedish Defense Research Agency, FOI, Linköping, Sweden. Tomas Bryllert is with Chalmers University of Technology, Göteborg, Sweden. N Llombart would like to thank the European Research Council for the starting grant LAA-THz-CC (639749). The authors would like to thank the European Defense Agency (EDA) for the support to this work in the context of the project TIPPSI (THz Imaging Phenomenology Platforms for Standoff IED Detection) funded by Germany, Netherlands, Poland and Sweden in the frame of the Project no B-1337-IAP1-GP of the European Defence Agency.

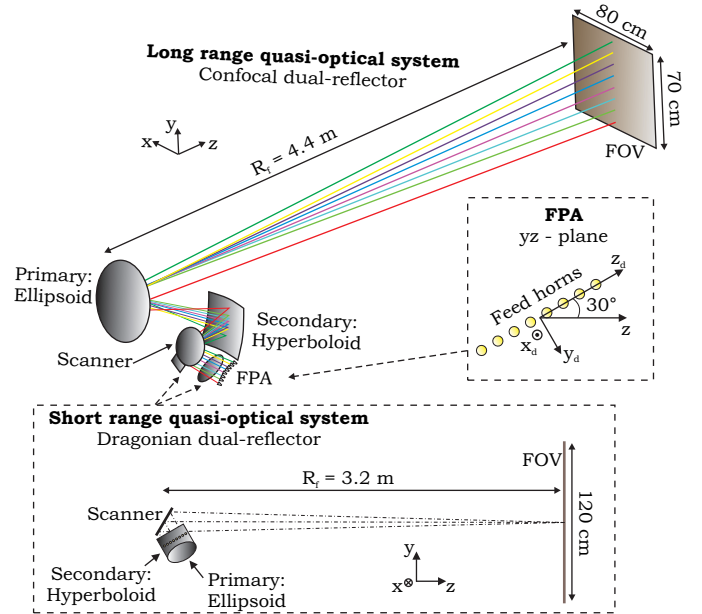


Fig. 1. Schematic representation of stand-off quasi-optical systems in different scenarios: confocal dual-reflector architecture for long range (narrow resolution) illuminated by a side fed Dragonian dual-reflector architecture used for short range (large resolution).

and synthetic imaging can be degraded by moving persons. Sub-millimeter wavelengths have emerged, instead, to be a good solution for people screening at larger stand-off distance, because relatively small physical apertures can achieve the required resolution. Moreover, the signal penetration through the clothing is still sufficient for detection at these frequencies.

Several sub-millimeter wave imagers are currently available in the literature [3]–[11], using passive or active schemes. Table I summarizes the current state-of-the-art of these systems. They are all based on an opto-mechanical antennas coupled to small focal plane arrays (FPA), and therefore they rely on mechanical scanning to generate the image. The current sub-millimeter wavelength imagers suffer from low speeds and/or limited Field of Views (FOV) due to the lack of integrated array technology at these frequencies. Passive imagers have been demonstrated using up to approximately 100 cooled detectors [8]–[11]. Instead, the development of active sub-millimeter wave imagers has been focused on single pixel architectures [4]–[7]. In [12], it was demonstrated that it is possible to develop compact homodyne active transceivers with sufficient sensitivity for security imaging. This enables a route for submillimeter-wave FPAs with 10 to 20 coherent

TABLE I
COMPARISON OF STATE-OF-THE-ART STAND-OFF IMAGERS AT SUB-MILLIMETER WAVE FREQUENCIES. $\Delta\rho$ IS THE 3 dB BEAM SIZE, M IS THE OPTICAL MAGNIFICATION, f_i THE IMAGING SPEED, D_s IS THE DIAMETER OF THE SCANNER.

Reference	Imager type	FPA elements	Freq. (GHz)	$\Delta\rho$ (cm)	Range (m)	FOV (cm)	M	D_s (cm)	f_i (Hz)
[4]	Active	1	676.5	1.4	25	40 × 40	10	12	1.0
[5]	Active	1	350	1.4	5	150 × 250	1	50	0.1
[6]	Active	1	300	1.6	8	80 × 50	5.5	11	1.0
[8]	Passive	64	640	4	8	400 × 200	1	32	7.0
[9]	Passive	64	350	1 to 2	10 to 20	100 × 100	4.2	24	25.0
[10]	Passive	128	600	1.5	5	100 × 200	1	50	8.0
[11]	Passive	152	350	1	3 to 5	100 × 200	1	44	2.0

transceivers achieving quasi-video rates.

The use of submillimeter-wavelength imagers for concealed object detection on non-cooperative subjects is envisaged in the future to insure security and defense in various scenarios. Several sensors can be used to protect the same building or venue and they have to work at different distances from the target and with different resolutions. Since quasi-optical systems operating in the Fresnel or near-field region are needed to meet the requirements of resolution and operating distances in submillimeter wavelength imagers for security applications [13], the operational imaging distance is defined by the surface of the primary reflector (see Fig. 1). In particular, an elliptical reflector with a focus on the image plane is commonly used as the primary mirror to achieve diffraction limited beams at the center of the FOV [13]. Even if, to certain extent, it is possible to achieve mechanical refocusing [14], these systems cannot operate in different environments requiring significantly different focusing ranges and similar cross-range resolutions, because the use of the same mirror aperture while refocusing will lead to larger beams at larger distances. Therefore, in this contribution, we present a modular opto-mechanical system able to operate in two scenarios with different range requirements.

In a short range (< 4 m) system, inset of Fig. 1, the angular FOV to image a person is very large, making it difficult to achieve low antenna scanning loss. However, the diameter of the primary optics is relatively small allowing the use of a mechanical scanner after the main aperture. For the systems operating, instead, at large range (> 4 m), Fig. 1, the angular FOV is relatively small. However, large apertures are required to achieve satisfactory resolution. Therefore, an optical magnification is necessary to reduce the physical dimensions of the mechanical scanner. The challenge, in this case, is to design an optical system that guarantees good scanning performance for both the FPA and the scanner.

The optical system architecture is therefore dependent on the dimensions of the mechanical scanner. In this contribution, general formulas that allow to evaluate the practical limits of the effective FOV in opto-mechanical diffraction limited quasi-optical systems for a specific scanner dimension are presented. The effective FOV is defined in this contribution as the dimension of the image plane in which the quasi-optical system directivity has a difference of less than 3 dB with respect to the broadside directivity, guaranteeing an approximately constant cross-range resolution. The definition relates to the overall effect of the phase losses (comparable to

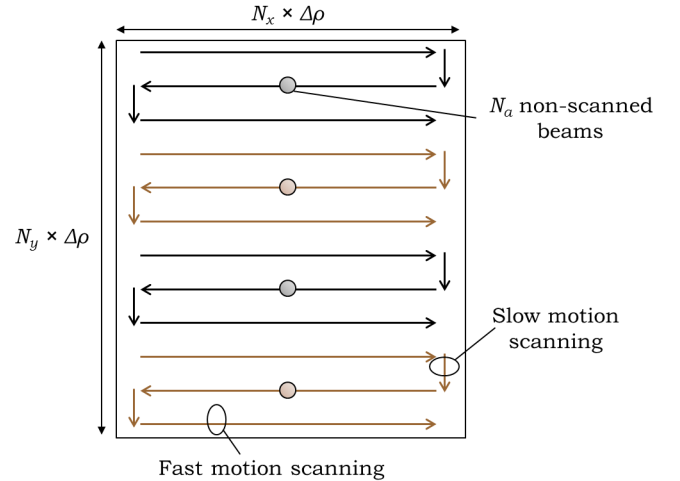


Fig. 2. Schematic representation of the beam scanning in the FOV using a raster scanning technique. N_x and N_y represent the number of points to be imaged in the horizontal and vertical direction, respectively; $\Delta\rho$ is the 3 dB beam size.

the Strehl ratio) effective aperture reduction and polarization losses. The effective FOV increases quadratically with the range distance and beam spot, and decreases significantly when a magnification is introduced to use a smaller scanner dimension. As an application example, we present the design of a dual-mode opto-mechanical system operating at 220 GHz. The system is based on a linear array of 8 homodyne transceivers [12].

The paper content is divided as follows. The practical trade-offs in designing the opto-mechanical systems together with the effective FOV as a function of the scanner diameter are described Sec. II. A compact reflector system that minimizes the scan loss for off-focus feeds is designed for a short range scenario as described in Sec. III. Also in Sec. III, the same architecture is coupled to a magnifying optical system for longer ranges. A prototype of the quasi-optical system was fabricated and is shown in Sec. IV along with its measurement results.

II. CANONICAL OPTO-MECHANICAL IMAGING SYSTEMS

The optimization of the opto-mechanical based imaging systems at sub-millimeter wavelengths is driven by two main parameters: the image resolution and the speed. The cross-range resolution is related to the half power beamwidth of the

field diffracted by the opto-mechanical system at the image plane and ultimately limits the effective FOV of an imaging system. The speed is related to how fast the imager can sample the FOV. In general, the image acquisition speed can be increased by using an FPA, because several points are imaged simultaneously. An FPA architecture for small arrays that leads to a well-sampled image at high speed is a sparse linear array of N_a elements with a raster scan [15]. In this case, a two axis scanning mechanism is required, as shown in Fig. 2, with one axis operating at a significantly higher speed given by

$$f_s = f_i \frac{N_y}{N_a} \quad (1)$$

where f_i is the required frame rate and N_y is the number of required pixels in the slow motion direction.

The maximum operational speed is imposed by the available mechanical scanner, which tends to be significantly slower the larger its physical dimension and the FOV size. In practice, the size of the scanner also determines the effective FOV. The optical architecture indeed depends on the diameter of the scanner, D_s , and how it compares to the main optics diameter, D_m . The latter is related to the range, R_f , the required 3 dB antenna beamwidth at the stand-off range, $\Delta\rho$, and the wavelength, λ_0 ,

$$D_m = 1.169 \frac{\lambda_0}{\Delta\rho} R_f \quad (2)$$

for -11 dB reflector edge illumination. This taper represents the best trade-off to maximize the aperture illumination efficiency with standard feeds [16].

Two scenarios can be identified depending on the ratio D_m/D_s . The optimum optical system architecture differs significantly in these two cases, named short range for $D_m/D_s < 1$, and large range for $D_m/D_s > 1$.

In this section, the effective FOV that can be achieved in these two scenarios by a canonical ideal optical system is evaluated. The figure of merit (effective FOV) is the 3 dB scan loss FOV (i.e. a directivity reduction of the last pixel of 3 dB with respect to the central one) as a function of the range and required resolution. The scan loss is evaluated considering the field radiated by the quasi-optical system, making the analysis general for active and passive imagers. This figure is useful to evaluate the performance of the proposed optical systems and the corresponding imaging quality of the imager. Indeed, a 3 dB scan loss corresponds roughly to a cross-range resolution enlargement of a factor 1.5, regardless of the type of imager (active or passive). If this condition is imposed, comparable resolution is achieved over the entire FOV, guaranteeing essentially the same image quality.

If the cross-range resolution, $\Delta\rho$, and the stand-off distance, R_f , are fixed, the diameter of the quasi-optical system can be calculated according to Eq. (2). As it was shown in [17], the effective FOV does not depend on the frequency of operation of the imaging system for a given combination of cross-range resolution and range. Therefore, the results presented in this section can be considered as a practical metric for the design of diffraction limited reflector systems for near-field focusing at sub-millimeter wavelengths. In particular, we consider an illumination of -11 dB of the reflector rims. Since ideal

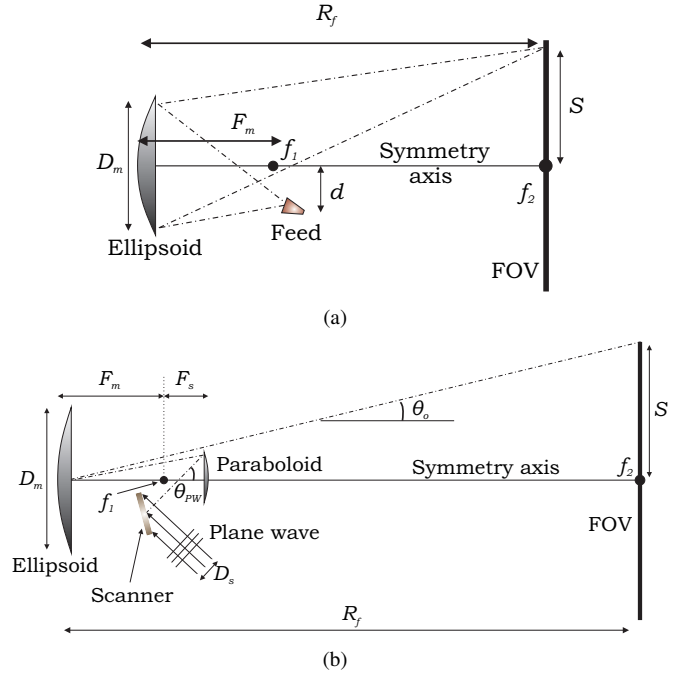


Fig. 3. Canonical reflector geometries considered in the analysis: (a) symmetric elliptical reflector and (b) symmetric confocal dual-reflector.

symmetric reflectors are considered, they actually represent the upper limits of the effective FOV of practical opto-mechanical systems implemented using offset reflector architectures with canonical surfaces. Indeed, all optical systems summarized in Table I are limited by the curves presented here.

A. Effective FOV limits for short range scenario

For short ranges, the scanner can be placed after the main optics in the transmit path (i.e. between the optics and the FOV) and has an impact in terms of spillover and image spatial sampling. However, it does not introduce additional phase aberrations. Therefore, the effective FOV is only limited by the quality of the patterns radiated by the FPA. In order to evaluate the effective FOV, one can consider a canonical symmetric elliptical reflector as in Fig. 3(a) with a flat scanner located after the focusing mirror (not shown in the figure for simplicity). The two foci of the ellipse, f_1 and f_2 , coincide with the center of the focal plane and the center of the FOV, respectively. The field radiated by a source in the focus f_1 is then focused in the focus f_2 and the corresponding radiation pattern is diffraction limited. The ratio between the focal distance, F_m , and the diameter, D_m , is referred as the f-number of the reflector, $f_{\#} = F_m/D_m$. If a feed is displaced in the focal plane of a quantity d from its center, the beam scattered by the reflector is linearly scanned in the FOV by a quantity S . The effective FOV is defined here as twice the scanning range (for symmetry), $2S$, for which the scan loss (i.e. gain reduction with respect to the gain of the on axis feed) reaches the value of 3 dB.

The variation, as a function of the imaging distance, of the effective FOV of the symmetric ellipse is plotted in Fig. 4(a), gray curves. The curves were obtained by using GRASP [18]

with the feeds tilted towards the center of the reflector. In such configuration, the spillover is negligible, and therefore the scan loss is mainly related to phase aberrations. To keep the same 3 dB beam size, $\Delta\rho$, while increasing the range, the diameter of the reflector has to be enlarged using Eq. (2). The corresponding values of D_m are reported in the top horizontal axis for $\Delta\rho = 1.4$ cm. The effective FOV size can be increased by enlarging the optical f-number of the reflector, $f_{\#}$. However, a very large f-number corresponds to a very large FPA to image a required FOV and can cause spillover problems [17]. Therefore, for practical reasons, an f-number between 2 and 3 is usually chosen when designing this kind of imagers. In the case of Fig. 4(a), it is fixed to $f_{\#} = 2.5$. Note that, in order to keep $f_{\#}$ constant, the focal distance, F_m , is changed according to the diameter while increasing the range.

The effective FOV increases as a function of the imaging distance, the spatial resolution and the f-number. Following a similar approach as in [19], a formula to describe the effective FOV by an elliptical reflector with -11 dB taper was derived by performing a parametric study in GRASP:

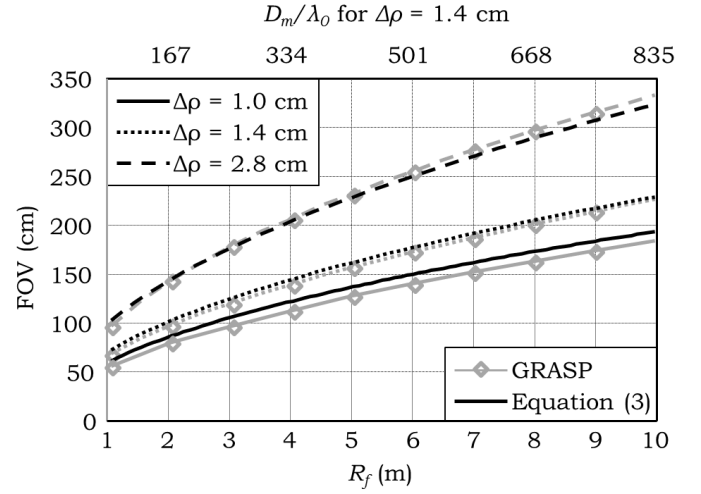
$$FOV_{SR}^e \approx 4.5\sqrt{R_f\Delta\rho^3}/\sqrt[3]{f_{\#}} \quad (3)$$

Eq. (3) was derived for: $1 \text{ m} \leq R_f \leq 10 \text{ m}$; $1 \text{ cm} \leq \Delta\rho \leq 5 \text{ cm}$; $2 \leq f_{\#} \leq 4$. Note that this ranges include most of the systems reported in Table I, with the exceptions of [4] and [9]. Therefore, it constitutes a relevant practical metric. For validation, it is also plotted in Fig. 4(a) (black curves) for the analyzed cases. The effective FOV predicted by Eq. (3) shows an agreement within 10 cm difference to the curves obtained in GRASP.

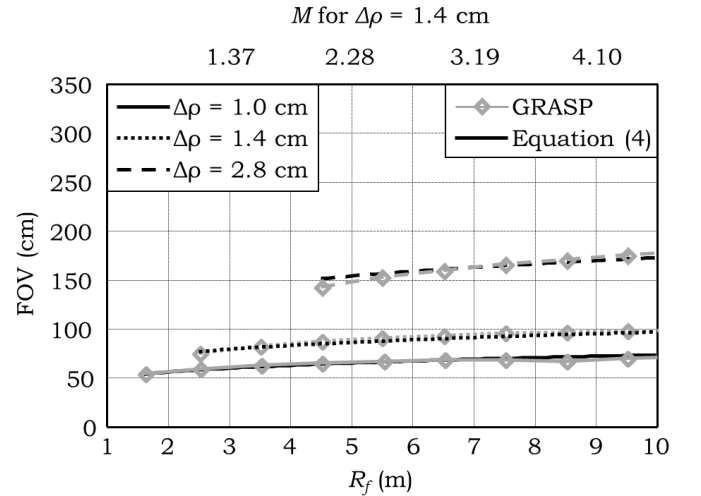
The possibility of using the described configuration depends on the size of the available scanner, D_s , that is typically fixed for mechanical reasons (i.e. maximum weight to achieve a desired speed). In particular, the scanner can be placed after the main aperture only if $D_m < D_s$. For example, considering a frequency of 220 GHz, $\Delta\rho = 1.4$ cm and $D_s = 25$ cm, this scenario is only applicable for $R_f < 2.2$ m. If this condition is not satisfied, an optical magnification has to be used so that the secondary optics has a size comparable to the one of the scanner.

B. Effective FOV limits for long range scenario

A reflector solution that was found to be efficient for security imagers based on mechanical scanners is the confocal architecture [13], [19]. The latter is shown in Fig. 3(b) in a symmetric arrangement. It is composed by a parabolic secondary mirror and an elliptical primary optics to focus in the near field. The confocal point f_1 is a common focus of both the secondary and primary mirrors. A plane wave impinging parallel to the optical axis on the parabolic reflector is focused in f_1 . The corresponding beam illuminating the elliptical primary mirror is then focused in the second focus of the ellipse, f_2 , that corresponds to the center of the FOV. If a plane wave impinges on the secondary mirror at an angle θ_{PW} , the field in the FOV is scanned to an angle $\theta_o \approx \theta_{PW}/M$, where M is the optical magnification and can be expressed as the ratio of the focal length of the two mirrors: $M = F_m/F_s$,



(a)



(b)

Fig. 4. Effective FOV as a function of the imaging distance for the described canonical reflector architectures: (a) symmetric elliptical reflector, (b) symmetric confocal dual-reflector.

with F_m and F_s shown in Fig. 3(b). Considering that the two mirrors have the same f-number, $F_m/D_m = F_s/D_s$, the magnification can be also expressed as $M = D_m/D_s$. The angular scan θ_o corresponds to the linear quantity S in Fig. 3(b). The same effect can be achieved by using a flat scanner before the secondary mirror illuminated by a collimated field and rotated of a quantity $\theta_{PW}/2$. As it was shown in [19], it is possible to calculate the position of the scanner that minimizes the spillover. Using this technique, the system scan performance is only limited by phase aberrations. The secondary reflector has to be oversized in order to intercept the beams deflected by the scanner. This configuration was used to estimate the performance of the canonical optical system considered here. The effective FOV of the confocal calculated by using GRASP is shown Fig. 4(b) (gray curves) for the same resolution values as for the symmetric ellipse of Sec. II-A and an f-number $f_{\#} = 1.5$. As an example, the

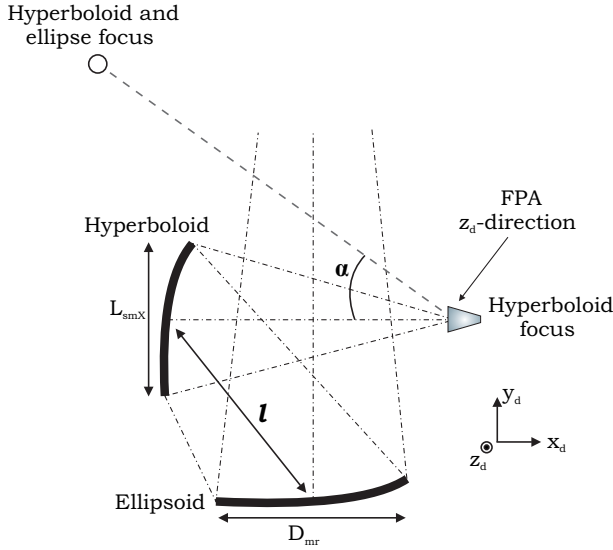


Fig. 5. Configuration and design parameters of the Dragonian dual-reflector system.

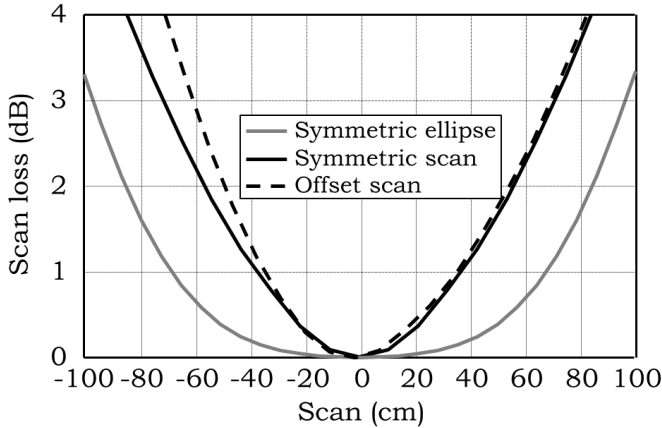


Fig. 6. Scan loss of the Dragonian dual-reflector architecture. The symmetric and offset scans refer to the field displacements in the z and x -directions, respectively.

diameter of the incident plane wave (and then the scanner) is fixed to $D_s = 183\lambda_0$, corresponding to 25 cm at 220 GHz. The confocal magnification, $M = D_m/D_s$, is varied with the range to keep the same plane wave dimension and cross-range resolution and it is indicated in the top horizontal axis of the figure. Note that the curves for different resolutions starts from different ranges, corresponding to the points in which the magnification is equal to one. By performing a parametric study in GRASP, the effective FOV of the confocal system can be approximated as

$$FOV_{LR}^e \approx 3.5 \frac{\sqrt{R_f \Delta \rho f_{\#}}}{\sqrt[3]{M}} \quad (4)$$

This equation is plotted in Fig. 4(b) (black curves) for comparison, showing excellent agreement with the GRASP simulations. Eq. (4) was derived for: $2.2 \text{ m} \leq R_f \leq 10 \text{ m}$; $1 \text{ cm} \leq \Delta \rho \leq 3 \text{ cm}$; $1 \leq f_{\#} \leq 2$; $1 \leq M \leq 7$. The effective

FOV of the confocal system is smaller than the one of the symmetric ellipse because of a residual loss introduced by the combination of the two reflectors that increases with the magnification. The derived formulas can be used to estimate an upper limit for the evaluation of the effective FOV of practical diffraction limited reflector configurations designed for maximum directivity at broadside.

The effective FOV can be enlarged by using a bifocal configuration [19]. Two sharp foci can be achieved in the FOV at the price of a small phase aberration loss at broadside. This configuration can be approximated by using a best fit confocal solution. The latter consists in the optimization of the positions of the two reflectors, without changing the mirror shapes, and allows a 50% effective FOV enlargement.

III. DUAL MODE OPTO-MECHANICAL PRACTICAL IMPLEMENTATION

In this section, a practical implementation of an opto-mechanical system suited for linear FPAs is described. It can operate in the two scenarios presented in Sec. II and is based on a modular approach: a short range scenario based optical system that can be used as the tertiary optics of a long range-based optical system. In both configurations, a raster scan technique is used to sample the FOV, Fig. 2. A flat scanner is used for the fast axis motion and the slow motion is implemented by rotating the primary mirror of the of the short range system. The choice of using two separate scanners simplifies the mechanical implementation. Only a few beams have to be scanned in the slow motion direction to fill the gaps between the feeds, making the use of the primary reflector the most compact solution without compromising the beam quality.

A. Short range system

For the short range scenario, the design is focused on the choice of the quasi-optical system that guarantees the best performance when illuminated by an FPA comparable in size to the main optics. In [17], a comparison in terms of scan loss of standard reflector and lens architectures for near-field imaging systems at sub-millimeter wave frequencies was presented. Thanks to its small optical magnification, the side-fed Dragonian dual-reflector configuration [20], [21] (see Fig. 5) was shown to be the practical configuration that allows the largest effective FOV when illuminated by a FPA [17]. For this reason, it was chosen for the current design. The Dragonian dual-reflector system was designed by following the procedure described in [21]. Two parameters have to be fixed: the distance between the two mirrors, l , and the offset angle, α , Fig. 5. In the current design, these parameters were optimized to minimize the scan loss associated to off-focus displacement of the feeds.

The FPA can be disposed either in the symmetric (z_d in Fig. 5) or offset (y_d in Fig. 5) direction of the focal plane of the reflector. The scan loss simulated by using GRASP in the symmetric and offset planes are shown in Fig. 6 for the design range, $R_f = 3.5 \text{ m}$. For the current analysis, the reflectors of the Dragonian are not oversized and the

feed is tilted towards the center of the secondary reflector for every analyzed position. The scan loss of the symmetric elliptical reflector described in the previous section with the same resolution is also reported as reference. The 3 dB FOV of the symmetrical elliptical reflector is almost 2 m. Instead, due to its offset configuration, the effective FOV of the Dragonian system is reduced to approximately 1.4 m and 1.3 m for symmetric and offset scanning directions, respectively. Since the scan loss is comparable in the two directions, the choice of the optical system architecture was driven by the minimization of the spillover and the dimension of the scanner. The FPA in the symmetric direction allows to oversize the secondary mirror without encountering blockage effects. The spillover on the scanner can be reduced by properly selecting its distance from the main aperture and adjusting the tilt angle of the feeds. These two operations allow to direct the beams towards the center of the scanner, minimizing its dimensions.

Eight feeds disposed symmetrically in the z_d -direction (see Fig. 5) are used in the design and they are schematically shown in Fig. 7(a). The exact positions of the feeds were optimized to compensate the beam deviation factor of the system. With the proposed configuration, the feeds point towards the center of the scanner as shown schematically in Fig. 7(b), where the output directions of the beams corresponding to all the feeds are reported. The edge feeds do not point to the center of the scanner because they are tilted by 4° toward the center of the secondary reflector. The reason for this choice is that, if no tilt is implemented, the size of the primary mirror of the Dragonian would increase significantly to avoid spillover. Since this mirror has to be rotated to scan in the slow motion direction, its size has to be as small as possible.

The optimized geometrical details at the central frequency $f_0 = 220$ GHz are reported in Table II. The range from the primary mirror is 3.5 m, and the corresponding diameter for 2.8 cm beam size can be calculated by using (2) to be 19.9 cm. The primary mirror diameter in Table II corresponds to a 15% oversize. The scanner is placed at 30 cm distance after the primary reflector and it is tilted by 30° . Therefore, the imaging distance from the scanner to the FOV is reduced to 3.2 m (see Fig. 1). The secondary reflector was designed with a rectangular rim since the spillover mainly occurs in the symmetric plane, where the feeds are arranged. Thanks to the oversized reflectors, optimized scanner position and feed tilts, the spillover loss is lower than 0.6 dB for all the feeds and scanner rotation angles.

The radiation patterns corresponding to the eight feeds of the FPA are shown in Fig. 8 when the scanner is not rotated. The patterns are normalized to the gain of an elliptical symmetric reflector focusing at the same range and with the same resolution. The 3 dB beamwidth is narrower than 3 cm for all the feeds, indicating the good quality of the radiation patterns over the scan range of the FPA.

In order to scan the fields in the horizontal direction (x in the inset of Fig. 1), the scanner is rotated about a vertical axis, parallel to the y_d -direction in Fig. 5. The patterns in the FOV when the scanner is rotated $\pm 6.75^\circ$ are shown in Fig. 9. The FOV is wider than 1.2×1.2 m², and the HPBW is narrower than 3.1 cm over the entire scanned area, with a

TABLE II
DESIGN DETAILS OF THE DESCRIBED DRAGONIAN DUAL-REFLECTOR SYSTEM. THE PRIMARY REFLECTOR AND THE SCANNER HAVE A CIRCULAR RIM WITH DIAMETERS D_{mr} AND D_{sc} . THE SECONDARY REFLECTOR HAS SQUARED RIM WITH SIDE LENGTH L_{smX} AND L_{smY} .

R_f (cm)	$\Delta\rho$ (cm)	$f_{\#}$	l (cm)	α ($^\circ$)	D_{mr} (cm)	D_{sc} (cm)	$L_{smX} \times L_{smY}$ (cm ²)
320	2.8	2.5	22	25	23	23	20×24

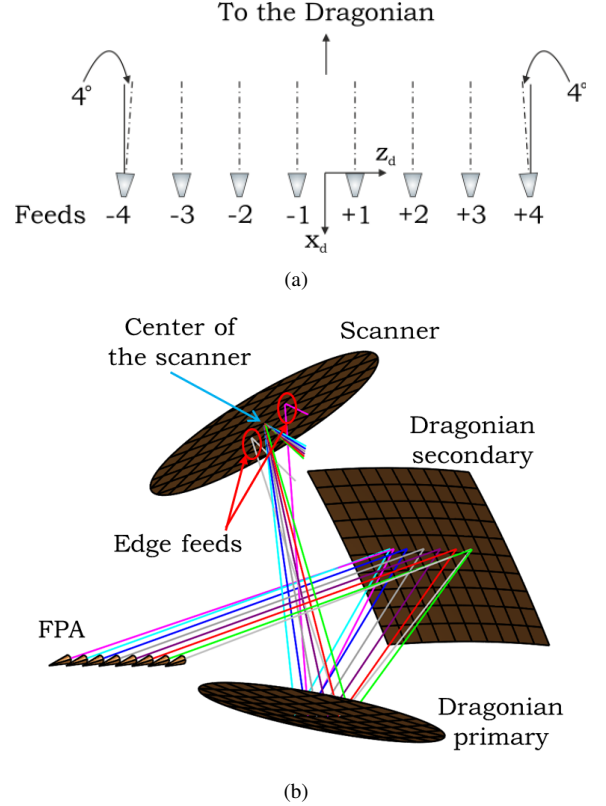


Fig. 7. System optimization details of the short range imager: (a) focal plane array, (b) output direction of the beams corresponding to the feeds.

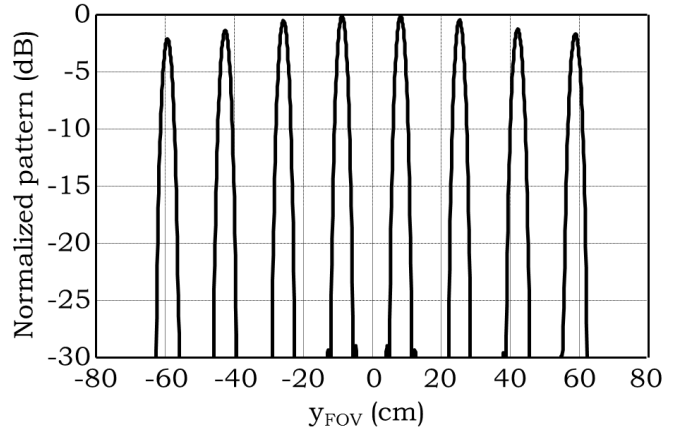


Fig. 8. Normalized radiation patterns at 220 GHz of the 8 feeds of the designed Dragonian reflector system.

TABLE III
DESIGN PARAMETERS OF THE CONFOCAL SYSTEM (SEE FIG. 10).

R_f (cm)	$\Delta\rho$ (cm)	$f_{\#}$	M	L_s (cm)	H_H (cm)	H_E (cm)	α ($^\circ$)	β ($^\circ$)
440	1.4	1.5	2	36	15.9	44.5	37	6.1

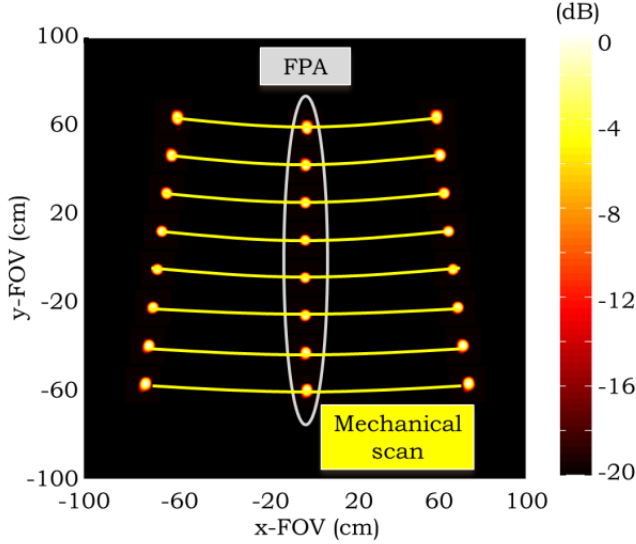


Fig. 9. Normalized radiation patterns of the designed Dragonian system in the xy -plane.

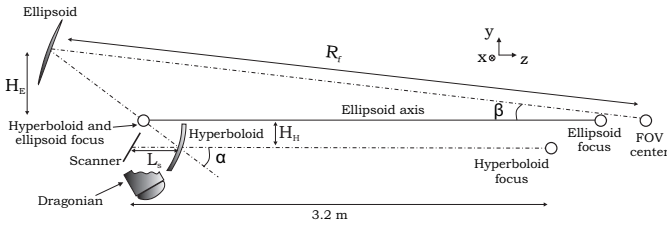


Fig. 10. Details of the designed confocal dual-reflector system.

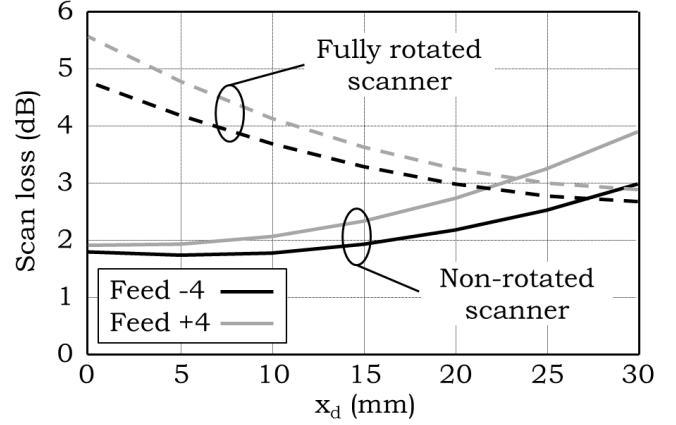
maximum scan loss of 2.2 dB. Note that, in this case, the FOV is limited by the size of the FPA and rotation range of the scanner and does not reach the limit of the effective FOV given in (3). The symmetric ellipse, for comparable scan loss, shows a FOV of $1.7 \times 1.7 \text{ m}^2$ (see Fig. 6). Therefore, the FOV of the optimized Dragonian system corresponds to 70% of the one of the canonical opto-mechanical system presented in Sec. II.

B. Long range system

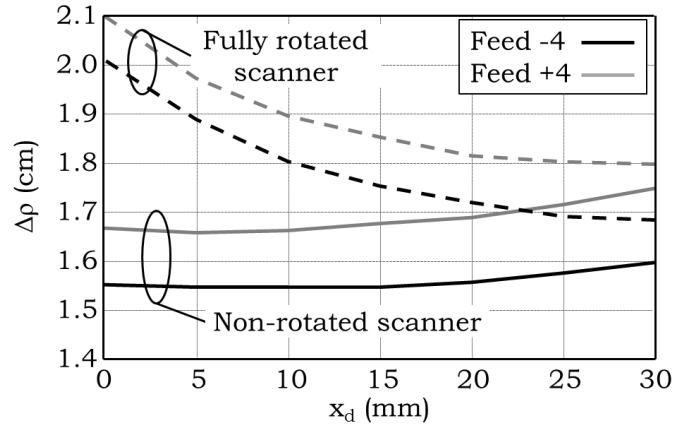
The Dragonian system described in Sec. III-A was used to illuminate a confocal dual-reflector system (see Fig. 1). The primary reflector of the system has a diameter of 50 cm and the focusing distance is 4.4 m. Therefore, according to Eq. (2), the 3 dB beam size is 1.4 cm. Even if the range is similar to the one of the quasi-optical system describe in Sec. III-A, the different design constraints of short and long range apply because of their different aperture sizes. The main reflector of

TABLE IV
OPTIMIZED POSITION AND TILTS OF THE FEEDS OF THE FPA.

Feed	z_d -position (mm)	x_d -position (mm)	Tilt ($^\circ$)
-4	-95.5	+20	4
-3	-65	+12	0
-2	-38.5	+3	0
-1	-13	0	0
+1	+13	0	0
+2	+36	+5	0
+3	+58.5	+14	0
+4	+80.5	+20	3.5



(a)



(b)

Fig. 11. Performance as a function of the x position of the feeds: (a) scan loss, (b) 3 dB beam size. The considered feeds are the edge ones, numbered ± 4 in Fig. 5(a).

the confocal system could be reshaped to achieve a different range. Instead, the sizes, shapes and positions of the other reflectors would not need to be changed.

Typically, the secondary reflector of a confocal system is a paraboloid and it is illuminated by a collimated beam [12], [19]. In the current design, the confocal system is illuminated by the Dragonian described in Sec. III-A that has an elliptical primary optics and an FPA. Therefore, a hyperbolic reflector is used as the secondary mirror of the confocal, Fig. 10. The hyperboloid has a focus coincident with the one of the primary

reflector of the confocal and one coincident with the center of the FOV of the Dragonian system. This mirror was oversized in the design to avoid spillover and has a rectangular rim, with side length $35 \times 35 \text{ cm}^2$. The details of the final design are shown in Fig. 10 and Table III. The confocal architecture was optimized to enlarge the effective FOV by using a bifocal configuration (see Sec. II-B). For this reason, the focus of the elliptical primary mirror and the center of the FOV do not coincide. A magnification $M = 2$ was used for the confocal system.

In the current configuration, the quadratic loss introduced by the confocal system [13] has to be optimized while the beam-scan occurs in both the symmetric and offset planes at the same time. In particular, the system is illuminated by the FPA in its offset plane and the scanner displaces the beams in the symmetric plane. The z_d -position of the feeds (see Fig. 7(a)) has to be optimized to keep into account the beam deviation factor. In order to improve the performance over the large considered FOV, the feeds have to be displaced also in the x_d -direction. The scan loss, including phase aberrations and spillover, of the edge feeds are shown in Fig. 11(a) as a function of their x_d -position. Note that in this analysis the feeds point towards the $-x_d$ -direction, i.e. no tilt is implemented. The tilt was included in a later stage to further reduce the spillover loss. The scan loss is shown for the cases of non-rotated and fully rotated scanner (8.2°). As the feeds are moved away from the secondary reflector of the Dragonian system (positive x_d -direction in Fig. 7(a)), the loss increases when the scanner is not rotated, whereas it reduces when the scanner is fully rotated. The same behavior can be observed in Fig. 11(b) for the 3dB beam size. These figures show that a trade-off between the performance with and without scanner rotation has to be done in order to achieve satisfactory scan loss and resolution over the entire FOV. Based on these considerations, all the feeds were optimized and their locations in the focal plane are reported in Table IV. As in the case of the short range scenario, all the feeds point to the center of the scanner with the exception of the edge ones that have to be tilted to reduce the spillover considering all the mirrors.

The patterns associated to the eight feeds of the FPA are shown in Fig. 12. They are normalized to the gain of an elliptical symmetric reflector focusing at the same range and with the same resolution. The patterns show a scan loss lower than 2.2 dB and the 3 dB beam size is narrower than 1.7 cm. The patterns in the xy -plane of the FOV are reported in Fig. 13, showing good quality over the entire scanning range. The slow motion needed to fill the gaps between the feeds is done by rotating the primary mirror of the Dragonian system, with a required rotation of $\pm 0.9^\circ$. The FOV is larger than $80 \times 70 \text{ cm}^2$ and the maximum scan loss is for feed +4 when both the scanner and the primary mirror of the Dragonian are fully rotated. The beam in this case points at -40.2 cm and $+45.6 \text{ cm}$ in the x and y -directions, respectively. The scan loss for this point is 4.2 dB and the 3 dB beam size is approximately 2 cm. Therefore, over the scanned FOV, the resolution enlargement is less than 1.5 times the required value (1.4 cm) and the spillover is lower than 1 dB.

In order to compare the results with the canonical archi-

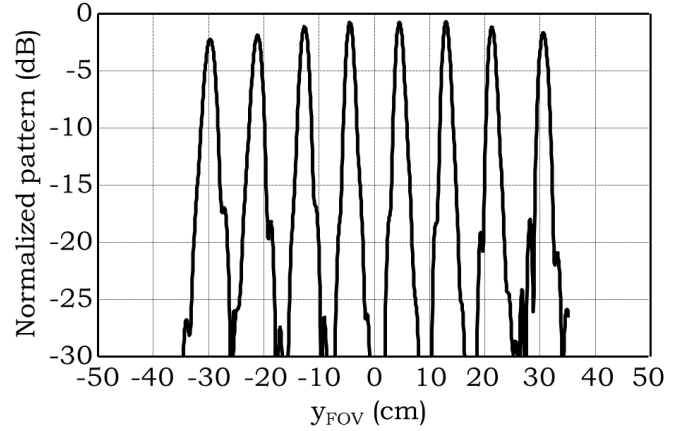


Fig. 12. Normalized radiation patterns of the confocal system at 220 GHz corresponding to the 8 feeds of the FPA.

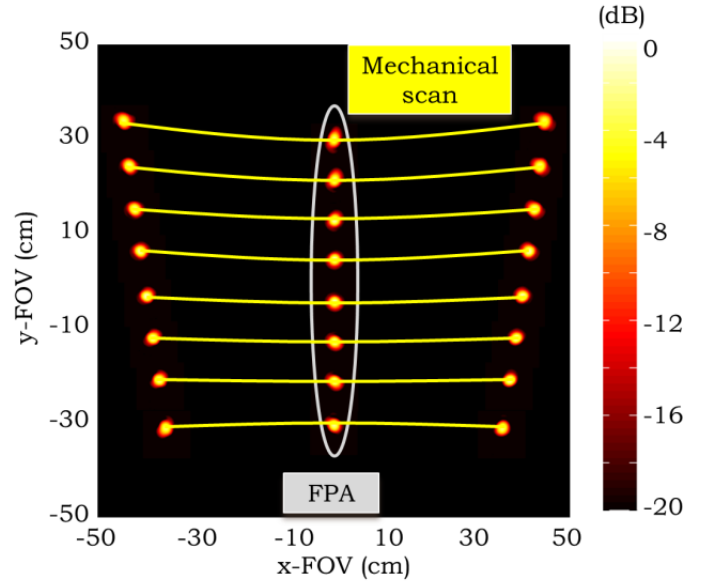


Fig. 13. Normalized radiation patterns at 220 GHz of the designed confocal system in the xy -plane.

ecture shown in Sec. II-B, only the area in which the scan loss is lower than 3 dB is considered. This corresponds to an effective FOV of $70 \times 70 \text{ cm}^2$. The symmetrical confocal system considered in Sec. II-B has a magnification of 2 for the considered range and resolution, corresponding to the current design. Note that the ratio between the diameter of the secondary and primary mirrors is not 2 because of the oversized diameter of the secondary reflector. The effective FOV shown in Fig. 3(b) for the canonical system is $85 \times 85 \text{ cm}^2$. Therefore, the effective FOV of the current design is approximately 70% of the one of the ideal architecture of Sec. II-B.

IV. PROTOTYPE FABRICATION AND MEASUREMENTS

The focusing mirrors of the optical systems described in Sec. III were fabricated and measured. The antenna patterns

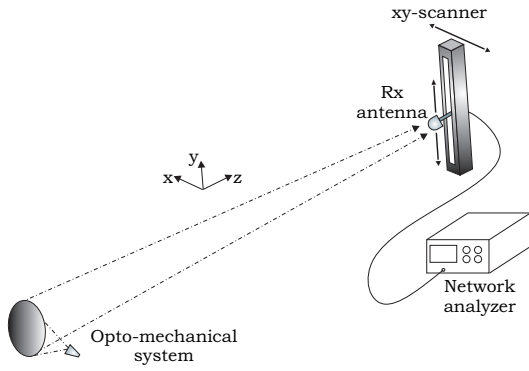


Fig. 14. Schematic representation of the measurement setup.

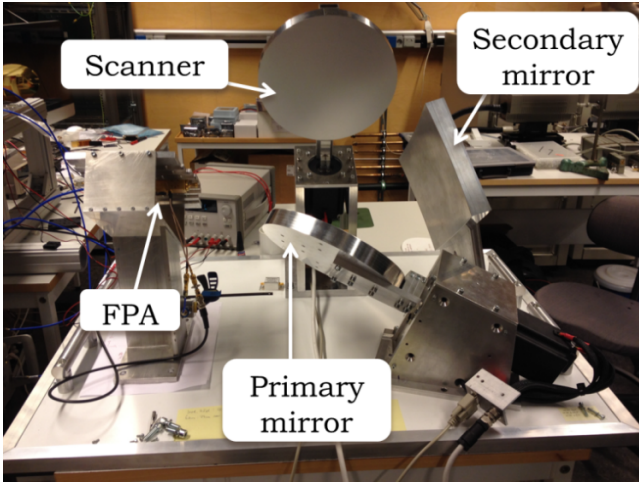
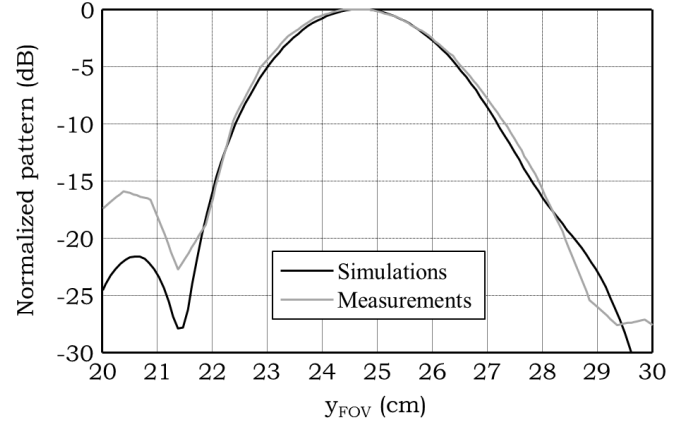


Fig. 15. Photograph of the prototype of the Dragonian system.

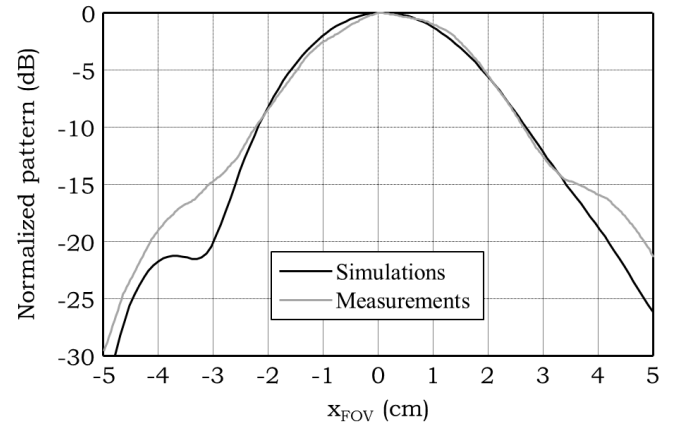
were measured using a near-field xy -scanner system, schematically shown in Fig. 14. The receiving antenna is a modified square-slot antenna positioned in the focus of an elliptical silicon lens with a 5.5 mm diameter [22]. The assembly of the Dragonian system is shown in Fig. 15 and is located at 3.2 m from the xy -scanner. A Custom Microwave conical horn RCH04R [23] was used to illuminate the optics. It provides a -10 dB taper at approximately 12° , as required by the chosen f-number of the Dragonian system ($f_{\#} = 2.5$). A low-weight implementation of the scanner is crucial to obtain fast scanning of the FOV. Therefore, the mirror was fabricated by using ALUCORE, an aluminum composite, as a material. This permitted to reduce its weight to less than 400 g and achieve a scanning speed of 10 Hz.

The patterns corresponding to several feeds of the FPA were measured and, as an example, the x and y cuts of the pattern of feed +2 (see Fig. 7(a)) are shown and compared to GRASP simulations in Fig. 16 at the central frequency $f_0 = 220$ GHz. Excellent agreement between measurements and simulations can be appreciated. The 3 dB beam size is approximately 2.8 cm, as predicted by the simulations, corresponding to a two-way resolution $\Delta\rho/\sqrt{2} = 2$ cm.

The Dragonian system was then used to illuminate the confocal dual-reflector architecture described in Sec. III-B for



(a)



(b)

Fig. 16. Measured radiation patterns at 220 GHz of the Dragonian system illuminated by feed +2: (a) x -direction, (b) y -direction.

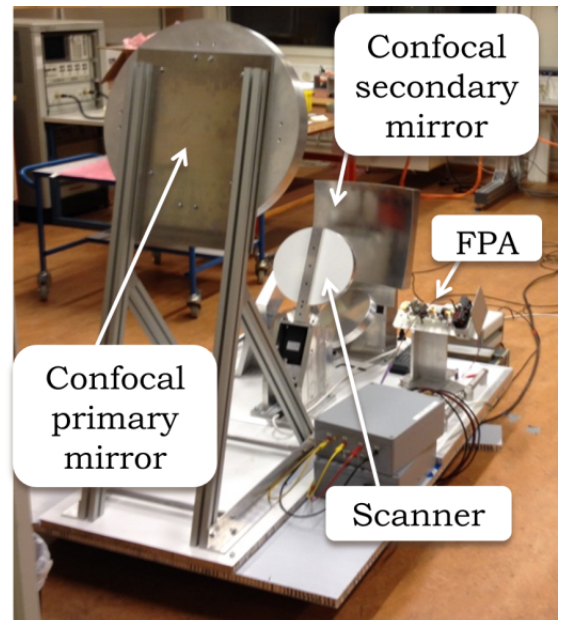


Fig. 17. Photograph of the prototype of the long range system.

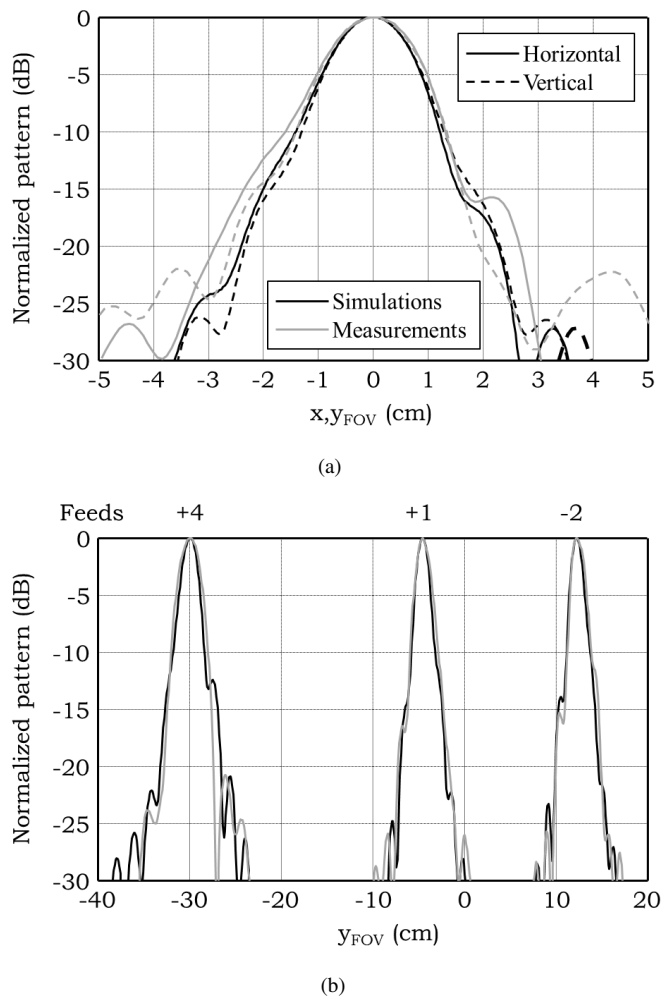


Fig. 18. Measured and simulated radiation patterns at 220 GHz of the confocal system described in Sec. III-B: (a) system illuminated in the center of the focal plane, (b) patterns corresponding to the feeds: -1 , $+2$, and $+4$. The black and red lines correspond to the simulation and measured results, respectively.

the long range scenario. A photograph of the system is shown in Fig. 17. As a first test, a feed was placed in the center of the focal plane. Its measured and simulated patterns in the FOV are shown in Fig. 18(a) in both the horizontal and vertical plane. Again, excellent agreement between measurements and simulations was found. The 3 dB beam size is approximately 1.4 cm as required and good pattern symmetry was achieved. The normalized patterns in the vertical plane corresponding to three feeds of the FPA, namely feeds -2 , $+1$ and $+4$ are shown in Fig. 18(b). The measured and simulated patterns are in good agreement. A slightly larger beam was achieved for the edge feed ($+4$). However, its HPBW is approximately 2.2, close to the requirement of maximum beam enlargement of a factor 1.5 (2.1 cm).

V. CONCLUSION

The practical limits of the effective FOV in opto-mechanical imaging systems at sub-millimeter wavelengths were described in details in terms of scan performance of canonical symmetric

reflector configurations. The effective FOV and optimal reflector configuration depends on the scanner physical dimensions, range and required spatial resolution. General equations that permit to predict the effective FOVs of diffraction limited reflector configurations with maximum directivity at broadside for any set of requirements were presented.

An implementation of such opto-mechanical system for a dual-mode stand-off imager at submillimeter wave illuminated by a linear focal plane array of eight active transceivers and using a raster scanning technique was presented and validated. For the short range scenario, a side-fed dual-reflector Dragonian system was identified among the most used offset reflector configurations as the one insuring the largest effective FOV when illuminated by an FPA. The scanner is arranged after the main aperture, without causing additional scan loss. The achieved field of view is $120 \times 120 \text{ cm}^2$ with a two-way resolution of 2 cm at 3.5 m range. The short range system was coupled to a magnified confocal dual-reflector system. The latter has a range similar to the one of the Dragonian system, but with a narrower resolution, maintaining the validity of the considerations for different optics apertures. In the optimization, the effect of the scanner was taken into account since it introduces additional phase aberration loss. In particular, the position of the feeds can be adjusted to guarantee a reasonable loss for the entire rotation range of the scanner. The effective FOV is $70 \times 70 \text{ cm}^2$ with a two-way resolution of 1 cm at 4.4 m range. The effective field of views of both operation modes of the system correspond to 70% of the effective FOVs achievable with canonical symmetric architectures. The experimental results confirmed the performance predicted by the simulations.

REFERENCES

- [1] www.3dx-ray.com.
- [2] www.sds.l-3com.com/products/advancedimagingtech.htm.
- [3] R. Appleby and H. B. Wallace, "Standoff detection of weapons and contraband in the 100 GHz to 1 THz region," *IEEE Trans. Antennas Propag.*, vol. 55, no. 11, pp. 2944-2956, Nov. 2007.
- [4] K.B. Cooper, R.J. Dengler, N. Llombart, T. Bryllert, G. Chattopadhyay, P. H. Siegel, "THz imaging radar for standoff personnel screening," *IEEE Trans. Terahertz Science Tech.*, vol. 52, no. 5, pp. 251-259, Sep. 2010.
- [5] D. Sheen, D. McMakin, T. Hall, and R. Severtsen, "Active millimeter-wave standoff and portal imaging techniques for personnel screening," *Proc. IEEE Conf. Technol. Homeland Security (HST 09)*, pp. 440-447, May 2009.
- [6] A. Garcia-Pino, B. Gonzalez-Valdes, O. Rubiños-Lopez, J. Grajal, A. Badolato, B. Mencia-Oliva, P. García Soidán, and J. L. Besada-Sanmartín, "Bifocal Reflector Antenna for a Standoff Radar Imaging System With Enhanced Field of View," *IEEE Trans. Antennas Propag.*, vol. 62, no.10, pp. 4997-5006, Oct. 2014.
- [7] C. A. Weg, W. von Spiegel, R. Henneberger, R. Zimmermann, T. Loeffler, and H. G. Roskos, "Fast active THz cameras with ranging capabilities," *J. Infrared Millimeter Terahertz Waves*, vol. 30, no. 12, pp. 1281-1296, Dec. 2009.
- [8] E. Grossman, C. Dietlein, J. Ala-Laurinaho, M. Leivo, L. Gronberg, M. Gronholm, P. Lappalainen, A. Rautiainen, A. Tamminen, and A. Luukanen, "Passive terahertz camera for standoff security screening," *Applied Optics*, vol. 49, no. 19, pp. E106-E120, Jul. 2010.
- [9] E. Heinz, T. May, D. Born, G. Zieger, K. Peiselt, V. Zakosarenko, T. Krause, A. Krüger, M. Schulz, F. Bauer, and H.-G. Meyer, "Progress in Passive Submillimeter-wave Video Imaging," *Proc. SPIE*, Jun. 2014.
- [10] A. Luukanen, J. Ala-Laurinaho, J. Häkli, D. Gomes-Martins, T. Kiuru, P. Koivisto, M. Leivo, A. Rautiainen, J. Säily, A. Tamminen, H. Toivanen, R. Tuovinen, and A. Räisänen, "Towards video rate imaging

at submillimetre-waves Finnish developments of passive multi-band imaging and holographic submmwave beam steering at VTT," *Proc. APMC*, Kaohsiung, Taiwan, Dec. 2012.

- [11] S. Rowe, E. Pascale, S. Doyle, C. Dunscombe, P. Hargrave, A. Papa-georgio, K. Wood, P. A. R. Ade, P. Barry, A. Bideaud, T. Brien, C. Dodd, W. Grainger, J. House, P. Mausekopf, P. Moseley, L. Spencer, R. Sudiwala, C. Tucker, and I. Walker, "A passive terahertz video camera based on lumped element kinetic inductance detectors," *AIP Review of Scientific Instruments*, 87, 033105-1, Mar. 2016.
- [12] T. Bryllert, V. Drakinskiy, K. B. Cooper, and J. Stake, "Integrated 200240-GHz FMCW radar transceiver module," *IEEE Trans. Microwave Theory Tech.*, vol. 61, no. 10, pp. 3808-3815, Oct. 2013.
- [13] N. Llombart, K. B. Cooper, R. J. Dengler, T. Bryllert, and P. H. Siegel, "Confocal ellipsoidal reflector system for a mechanically scanned active terahertz imager," *IEEE Trans. Antennas Propag.*, vol. 58, no. 6, pp. 1834-1841, Jun. 2010.
- [14] N. Llombart and B. Blazquez, "Refocusing a THz imaging radar: implementation and measurements," *IEEE Trans. Antennas Propag.*, vol. 62, no.3, pp. 1529-1534, Mar. 2014.
- [15] N. Llombart, R. J. Dengler, and K. B. Cooper, "Refocusing a THz imaging radar: implementation and measurements," *IEEE Antennas Propag. Magazine*, vol. 52, no.5, pp. 251-259, Oct. 2010.
- [16] P. F. Goldsmith, "Quasioptical systems: Gaussian beam quasioptical propagation and applications," Wiley-IEEE Press, ISBN: 978-0-7803-3439-7, 1997.
- [17] E. Gandini and N. Llombart, "Toward a real time stand-off submillimeter-wave imaging system with large field of view: quasioptical system design considerations," *Proc. SPIE*, vol. 9462, Apr. 2015.
- [18] TICRA GRASP-10.5.0.
- [19] A. Garcia-Pino, N. Llombart, B. Gonzalez-Valdes, and O. Rubiños-Lopez, "Terahertz antenna system for a near-video-rate radar imager," *IEEE Trans. Antennas Propag.*, vol. 60, no.9, pp. 4119-4129, Sep. 2012.
- [20] C. Dragone, "Unique reflector arrangement with very wide field of view for multibeam antennas," *Electron. Lett.*, vol. 19, no. 25/26, pp. 10611062, Dec. 1983.
- [21] S. Chang and A. Prata Jr., "The design of classical offset Dragonian reflector antennas with circular apertures," *IEEE Trans. Antennas Propag.*, vol. 52, no. 1, pp. 1219, Jan. 2004.
- [22] M. Abbasi, S. E. Gunnarsson, N. Wadefalk, R. Kozhuharov, J. Svedin, S. Cherednichenko, I. Angelov, I. Kallfass, A. Leuther, and H. Zirath, "Single-chip 220-GHz active heterodyne receiver and transmitter MMICs with on-chip integrated antenna," *IEEE Trans. Microwave Theory Tech.*, vol. 59, no. 2, pp. 466-478, Feb. 2011.
- [23] www.custommicrowave.com.



Erio Gandini received the M.Sc. degree in electrical engineering from the University of Modena and Reggio Emilia, Modena, Italy and the PhD degree in Electrical Engineering from the University of Rennes 1 in 2009 and 2012, respectively. In 2011 he was a visiting PhD student at the University of Michigan. In January 2013 he joined the Ecole polytechnique fédérale de Lausanne (EPFL), Lausanne, Switzerland. In October 2013 he joined the THz sensing group at the Delft University of Technology, Delft, the Netherlands, where he currently working

as research scientist. Since 2016 he is working as Antenna Scientist in the radar department of TNO Defence, Security and Safety, The Hague, The Netherlands. Erio Gandini scientific activities are in the broad area of applied electromagnetics. His research interests include quasi-optical systems, phased array antennas, sub-millimeter and terahertz imaging systems, frequency selective surfaces, beam-forming networks.



Jan Svedin (M88) received the M.Sc. degree in applied physics and electrical engineering and the Ph.D. degree in theoretical physics from the Linköping Institute of Technology, Linköping, Sweden, in 1986 and 1991, respectively. He joined the Swedish Defence Research Establishment (FOI), Linköping, in 1987 and is presently a Deputy Director of Research at the Radar Systems Department. His research interests are presently within the field of millimeter wave technology and its various applications, including antennas, components and

manufacturing technologies for sensor imaging systems.



Tomas Bryllert was born in Växjö, Sweden in 1974. He received the degree of M.S. in physics and the Ph.D. in semiconductor physics from Lund University, Lund, Sweden in 2000 and 2005 respectively. In 2006 he joined the Microwave Electronics Laboratory at Chalmers University of Technology, Göteborg, Sweden. From 2007-2009 Dr. Bryllert was with the Submillimeter Wave Advanced Technology (SWAT) group at the Jet Propulsion Laboratory, California Institute of Technology, Pasadena, USA. Dr Bryllert is currently with the Terahertz and

Millimetre Wave Laboratory at Chalmers University of Technology. He is also co-founder and Chief Executive Officer (CEO) of Wasa Millimeter Wave AB, a company that develops and fabricates millimeter wave products. His research interests are sub-millimeter wave electronic circuits and their applications in imaging- and radar systems.



Nuria Llombart (S06M07SM13) received the Electrical Engineering and Ph.D. degrees from the Polytechnic University of Valencia, Spain, in 2002 and 2006, respectively. During her Master's degree studies she spent one year at the Friedrich-Alexander University of Erlangen-Nuremberg, Germany, and worked at the Fraunhofer Institute for Integrated Circuits, Erlangen, Germany. From 2002 until 2007, she was with the Antenna Group, TNO Defence, Security and Safety Institute, The Hague, The Netherlands, working as a Ph.D. student and afterwards

as a Researcher. From 2007 until 2010, she was a Postdoctoral Fellow at the California Institute of Technology, working for the Sub millimeter Wave Advance Technology Group, Jet Propulsion Laboratory, Pasadena, USA. She was a Ramón y Cajal Fellow at the Optics Department of the Complutense University of Madrid, Spain, from 2010 to 2012. In September 2012, she joined the THz Sensing Group at the Technical University of Delft, The Netherlands, where she is currently an Associate Professor. She has co-authored over 150 journal and international conference contributions. Her research interests include the analysis and design of planar antennas, periodic structures, reflector antennas, lens antennas, and waveguide structures, with emphasis in the THz range. Dr. Llombart was co-recipient of the H.A. Wheeler Award for the Best Applications Paper of the year 2008 in the IEEE Transactions on Antennas and Propagation, the 2014 THz Science and Technology Best Paper Award of the IEEE Microwave Theory and Techniques Society and several NASA awards. She also received the 2014 IEEE Antenna and Propagation Society Lot Shafai Mid-Career Distinguished Achievement Award. In 2015, she was awarded with an European Research Council (ERC) Starting Grant. She currently serves as a Board Member of the IRMMW-THz International Society.